$[ReCl_4(CN)_2]^{2-}$: A High Magnetic Anisotropy Building Unit Giving Rise to the Single-Chain Magnets $(DMF)_4MReCl_4(CN)_2$ (M = Mn, Fe, Co, Ni)

T. David Harris,[†] Miriam V. Bennett,[†,‡] Rodolphe Clérac,*[,§,‖] and Jeffrey R. Long*[,†]

Department of Chemistry, University of California, Berkeley, California 94720, Department of Chemistry and Biochemistry, San Diego State University, San Diego, California 92182, CNRS, UPR 8641, Centre de Recherche Paul Pascal (CRPP), Equipe "Matériaux Moléculaires Magnétiques", 115 avenue du Dr. Albert Schweitzer, 33600 Pessac, France, and Université de Bordeaux, UPR 8641, Pessac F-33600, France

Received December 30, 2009; E-mail: clerac@crpp-bordeaux.cnrs.fr; jrlong@berkeley.edu

Abstract: An $S = {}^3/_2$, high-anisotropy building unit, *trans*-$[ReCl_4(CN)_2]^{2-}$, representing the first paramagnetic complex with a mixture of just cyanide and halide ligands, has been synthesized through the reaction of $(Bu_4N)CN$ with $ReCl_4(THF)_2$. This species is characterized in detail and employed in directing the formation of a series of one-dimensional coordination solids of formula $(DMF)_4MReCl_4(CN)_2$ (M = Mn (**2**), Fe (**3**), Co (**4**), Ni (**5**)). Variable-temperature dc magnetic susceptibility measurements demonstrate the presence of intrachain antiferromagnetic (**2**) and ferromagnetic (**3**−**5**) exchange coupling within these solids. In addition, probing the ac magnetic susceptibility as a function of both temperature and frequency reveals that all of the chain compounds exhibit slow relaxation of the magnetization. The relaxation time is shown to be thermally activated, with energy barriers to relaxation of $\Delta_\tau = 31, 56, 17,$ and 20 cm^{-1} for **2**−**5**, respectively. Notably, the field-dependent magnetization of the iron congener exhibits a significant hysteresis effect at low temperature, with a coercive field of $H_C = 1.0$ T, thus demonstrating magnetlike behavior in this one-dimensional system. Finally, the magnetization dynamics of all solids occur within the finite-size regime, where the magnetic domain growth is limited due to physical defects along the chains within the crystals.

Introduction

Nearly two decades ago, researchers discovered that certain molecules exhibit slow relaxation of the magnetization after removal of an applied dc magnetic field, a phenomenon stemming from an energy barrier to spin inversion.[1] Such species can thus behave at low temperature as classical magnets and have come to be known as single-molecule magnets. This discovery sparked much excitement, in part because single-molecule magnets could potentially find use in applications such as high-density information storage and quantum computing.[2] However, for such applications to be realized, dramatic increases in spin-reversal barriers must be achieved. Indeed, despite the tremendous effort directed toward this goal, the highest relaxation barrier yet reported for a molecule is 67 cm^{-1}, less than one-third the thermal energy available at room temperature.[1f]

In 2001, slow relaxation of the magnetization was observed in a one-dimensional solid,[3] a phenomenon predicted by Glauber over four decades ago.[4] This solid, a radical-bridged compound of formula $Co(hfac)_2(NITPhOMe)$, displays a relaxation barrier of 107 cm^{-1},[5] representing nearly a 2-fold increase over the current record in molecular systems. Such a remarkable energy barrier exists for this solid despite the modest net spin generated through antiferromagnetic coupling between anisotropic Co^{II} ions (effective $S = {}^1/_2$) and nitroxide radical ligands ($S = {}^1/_2$). Spurred by this breakthrough, many researchers have recently begun targeting other one-dimensional systems that exhibit slow relaxation of the magnetization,[6] which have come to be known as single-chain magnets.[6a] Indeed, the nascent field of single-chain magnet research has already seen the formation of several

[†] University of California.
[‡] San Diego State University.
[§] Centre de Recherche Paul Pascal (CRPP).
[‖] Université de Bordeaux.

(1) (a) Sessoli, R.; Tsai, H. L.; Schake, A. R.; Wang, S.; Vincent, J. B.; Folting, K.; Gatteschi, D.; Christou, G.; Hendrickson, D. N. *J. Am. Chem. Soc.* **1993**, *115*, 1804. (b) Sessoli, R.; Gatteschi, D.; Caneschi, A.; Novak, M. A. *Nature* **1993**, *365*, 141. (c) Gatteschi, D.; Sessoli, R.; Villain, J. *Molecular Nanomagnets*; Oxford University Press: New York, 2006, and references therein. (d) Milios, C. J.; Vinslava, A.; Wernsdorfer, W.; Moggach, S.; Parsons, S.; Perlepes, S. P.; Christou, G.; Brechin, E. K. *J. Am. Chem. Soc.* **2007**, *129*, 2754. (e) Freedman, D. E.; Jenkins, D. M.; Iavarone, A. T.; Long, J. R. *J. Am. Chem. Soc.* **2008**, *130*, 2884. (f) Yoshihara, D.; Karasawa, S.; Koga, N. *J. Am. Chem. Soc.* **2008**, *130*, 10460.

(2) (a) Garanin, D. A.; Chudnovsky, E. M. *Phys. Rev. B* **1997**, *56*, 11102. (b) Leuenberger, M. N.; Loss, D. *Nature* **2001**, *410*, 789. (c) Heersche, H. B.; de Groot, Z.; Folk, J. A.; van der Zant, H. S. J.; Romeike, C.; Wegewijs, M. R.; Zobbi, L.; Barreca, D.; Tondello, E.; Cornia, A. *Phys. Rev. Lett.* **2006**, *96*, 206801. (d) Jo, M.-H.; Grose, J. E.; Liang, W.; Baheti, K.; Deshmukh, M. M.; Sokol, J. J.; Rumberger, E. M.; Hendrickson, D. N.; Long, J. R.; Park, H.; Ralph, D. C. *Nano Lett.* **2006**, *6*, 2014.

(3) Caneschi, A.; Gatteschi, D.; Lalioti, N.; Sangregorio, C.; Sessoli, R.; Venturi, G.; Vindigni, A.; Rettori, A.; Pini, M. G.; Novak, M. A. *Angew. Chem., Int. Ed.* **2001**, *40*, 1760.

(4) Glauber, R. J. *J. Math. Phys.* **1963**, *4*, 294.

(5) A wavenumber as a unit of energy is related to degrees Kelvin through the following expression: $E(\text{cm}^{-1})/k_B = E(K)$, where k_B is the Boltzmann constant, such that 1 cm^{-1} = 1.44 K.

new one-dimensional materials exhibiting relaxation barriers higher than any yet observed in single-molecule magnets.[3,6b−d,i]

The increase in relaxation barrier for single-chain magnets over their molecular counterparts can be attributed to an added energy component to the overall barrier in one-dimensional systems. In single-molecule magnets, the energy barrier, Δ_A, stems from a uniaxial magnetic anisotropy, D, acting on a high-spin ground state, S, such that $\Delta_A = S^2|D|$ for integer S values or $\Delta_A = (S^2 - \frac{1}{4})|D|$ for half-integer S values (according to the Hamiltonian $H = DS_z^2$, where S_z is the component of S along the z direction). The same anisotropy energy barrier is also present in single-chain magnets, where each chain is composed of individual repeating anisotropic spin units.[7] In addition to this anisotropy barrier, however, single-chain magnets experience an added component to the overall relaxation barrier that stems from short-range magnetic correlation along each individual chain. The length of this correlation, ξ, increases exponentially as the temperature is lowered, where infinite chains are divided into domains of length $L = 2\xi$.[8] As such, inverting a spin within a chain requires the creation of two new domain walls. This added energy requirement for inverting the magnetization, not present in molecules, is known as the correlation energy, Δ_ξ, and corresponds physically to the energy required to create a domain wall. Thus, the total energy required to invert the magnetization in a single-chain magnet, Δ_τ, may be expressed as $\Delta_\tau = 2\Delta_\xi + \Delta_A$.[6f] This relationship, however, only provides a valid measure of the relaxation barrier within a regime where the chain can be considered infinite. At very low temperatures, the correlation length becomes arrested by defects within the solid.[9] In this finite-size regime, the total energy needed to invert the magnetization reduces to $\Delta_\tau = \Delta_\xi + \Delta_A$, since the reversal of the magnetization becomes more probable from the ends of the finite-size chains.[6f,7] Indeed, previous investigations into the magnetization dynamics of single-chain magnets have found relaxation processes in a single compound corresponding to both infinite- and finite-size regimes by studying the relaxation time in a broad temperature range.[6k,7] One-dimensional chain structures with exchangeable components[10] could provide an important means of probing such effects, while also facilitating variation of anisotropy and magnetic exchange as a means of enhancing the relaxation barrier.

Our approach to synthesizing modular single-chain magnets of this type was initiated through the synthesis of a paramagnetic building unit well-suited for directing the formation of one-dimensional coordination solids. Rhenium(IV) was selected as a metal center owing to its $S = \frac{3}{2}$ spin ground state (in an octahedral coordination environment) and the large magnetic anisotropy arising from spin−orbit coupling associated with the third-row transition ion. Indeed, previous studies have reported extremely large axial zero-field splitting parameters for mono-nuclear rhenium(IV) complexes,[11] as high as $D = 53$ cm^{-1} for $[ReCl_4(ox)]^{2-}$.[11b] Moreover, the building unit $[ReCl_4(ox)]^{2-}$ has been successfully incorporated into a NiRe$_3$ cluster that exhibits single-molecule magnet behavior at low temperature.[12] In addition, for directing the formation of a one-dimensional chain structure, a complex featuring only two trans terminal cyanide ligands is desirable. Here, we introduce just such a building unit, with the preparation of the high-anisotropy $S = \frac{3}{2}$ complex *trans*-$[ReCl_4(CN)_2]^{2-}$, the first structurally characterized example of a paramagnetic molecule of the form $[MX_x(CN)_y]^{n-}$ ($X^- =$ halide). Additionally, we report the successful incorporation of this complex into a series of cyano-bridged one-dimensional coordination solids $(DMF)_4MReCl_4(CN)_2$ (M = Mn, Fe, Co, Ni), all exhibiting slow relaxation of the magnetization.

Experimental Section

Preparation of Compounds. The compounds *cis*-[ReCl$_4$-(THF)$_2$][13] and (Bu$_4$N)CN[14] were synthesized according to literature procedures. Solid (Bu$_4$N)CN was dried in vacuo ($P < 10^{-3}$ Torr) for 36 h using a trap containing P$_2$O$_5$ prior to use. All other reagents were obtained from commercial sources and used without further purification. Compound **1** was prepared under a dinitrogen atmosphere using standard glovebox techniques. *Caution!* Although we have experienced no problems while working with them, perchlorate salts are potentially explosive and should be handled with extreme care and only in small quantities.

(Bu$_4$N)$_2$[*trans*-ReCl$_4$(CN)$_2$]·2DMA (1). Under an atmosphere of dinitrogen, solid (Bu$_4$N)CN (0.41 g, 1.5 mmol) was added to a stirred green solution of *cis*-[ReCl$_4$(THF)$_2$] in 2 mL of DMF. The resulting dark brown viscous solution was stirred for 24 h and then exposed to air. Addition of 25 mL of water to the solution resulted in the formation of a brown precipitate. The precipitate was collected by filtration, washed with water (3 × 25 mL), and allowed to dry on the filter for 30 min. The pale brown solid was then dissolved in 1.5 mL of *N,N*-dimethylacetamide (DMA), and the resulting dark yellow solution was filtered through diatomaceous earth. Diffusion of diethyl ether vapor into the resulting filtrate yielded 0.20 g (44%) of pale blue rod-shaped crystals suitable for

(6) (a) Clérac, R.; Miyasaka, H.; Yamashita, M.; Coulon, C. *J. Am. Chem. Soc.* **2002**, *124*, 12837. (b) Lescouëzec, R.; Vaissermann, J.; Ruiz-Pérez, C.; Lloret, F.; Carrasco, R.; Julve, M.; Verdaguer, M.; Dromzée, Y.; Gatteschi, D.; Wernsdorfer, W. *Angew. Chem., Int. Ed.* **2003**, *42*, 1483. (c) Liu, T. F.; Fu, D.; Gao, S.; Zhang, Y. Z.; Sun, H. L.; Su, G.; Liu, Y. J. *J. Am. Chem. Soc.* **2003**, *125*, 13976. (d) Wang, S.; Zuo, J.-L.; Gao, S.; Song, Y.; Zhou, H.-C.; Zhang, Y.-Z.; You, X.-Z. *J. Am. Chem. Soc.* **2004**, *126*, 8900. (e) Ferbinteanu, M.; Miyasaka, H.; Wernsdorfer, W.; Nakata, K.; Sugiura, K.; Yamashita, M.; Coulon, C.; Clérac, R. *J. Am. Chem. Soc.* **2005**, *127*, 3090. (f) Coulon, C.; Miyasaka, H.; Clérac, R. *Struct. Bonding (Berlin)* **2006**, *122*, 163. (g) Bernot, K.; Bogani, L.; Caneschi, A.; Gatteschi, D.; Sessoli, R. *J. Am. Chem. Soc.* **2006**, *128*, 7947. (h) Miyasaka, H.; Madanbashi, T.; Sugimoto, K.; Nakazawa, Y.; Wernsdorfer, W.; Sugiura, K.; Yamashita, M.; Coulon, C.; Clérac, R. *Chem. Eur. J.* **2006**, *12*, 7028. (i) Xu, H.-B.; Wang, B.-W.; Pan, F.; Wang, Z.-M.; Gao, S. *Angew. Chem., Int. Ed.* **2007**, *46*, 7388. (j) Ishii, N.; Okamura, Y.; Chiba, S.; Nogami, T.; Ishida, T. *J. Am. Chem. Soc.* **2008**, *130*, 24. (k) Miyasaka, H.; Julve, M.; Yamashita, M.; Clérac, R. *Inorg. Chem.* **2009**, *48*, 3420, and references therein. (l) Coulon, C.; Clérac, R.; Wernsdorfer, W.; Colin, T.; Miyasaka, H. *Phys. Rev. Lett.* **2009**, *102*, 167204.
(7) Coulon, C.; Clérac, R.; Lecren, L.; Wernsdorfer, W.; Miyasaka, H. *Phys. Rev. B* **2004**, *69*, 132408.
(8) Loveluck, J. M.; Lovesey, S. W.; Aubry, S. *J. Phys. C: Solid State Phys.* **1975**, *8*, 3841.
(9) (a) Imry, Y.; Montano, P. A.; Hone, D. *Phys. Rev. B* **1975**, *12*, 253. (b) Leal de Silva, J. K.; Moreira, A. G.; Soares, M. S.; Sá Barreto, F. C. *Phys. Rev. B* **1995**, *52*, 4527. (c) Luscombe, J. H.; Luban, M.; Reynolds, J. P. *Phys. Rev. E* **1996**, *53*, 5852.

(10) Bernot, K.; Bogani, L.; Caneschi, A.; Gatteschi, D.; Sessoli, R. *J. Am. Chem. Soc.* **2006**, *128*, 7947.
(11) (a) Tomkiewicz, A.; Villain, F.; Mrozinski, J. *J. Mol. Struct.* **2000**, *555*, 383. (b) Tomkiewicz, A.; Bartczak, T. J.; Kruszynski, R.; Mrozinski, J. *J. Mol. Struct.* **2001**, *595*, 225. (c) Martínez-Lillo, J.; Armentano, D.; De Munno, G.; Lloret, F.; Julve, M.; Faus, J. *Inorg. Chim. Acta* **2006**, *359*, 4343.
(12) (a) Martínez-Lillo, J.; Armentano, D.; De Munno, G.; Wernsdorfer, W.; Julve, M.; Lloret, F.; Faus, J. *J. Am. Chem. Soc.* **2006**, *128*, 14219. (b) Martínez-Lillo, J.; Armentano, D.; De Munno, G.; Wernsdorfer, W.; Clemente-Juan, J. M.; Krzystek, J.; Lloret, F.; Julve, M.; Faus, J. *Inorg. Chem.* **2009**, *48*, 3027.
(13) Allen, E. A.; Johnson, N. P.; Rosevear, D. T.; Wilkinson, W. *J. Chem. Soc.* **1969**, 788.
(14) Kobler, H.; Munz, R.; Al Gasser, G.; Simchen, G. *Justus Liebigs Ann. Chem.* **1978**, 1937.

Table 1. Crystallographic Data[a] for $(Bu_4N)_2[ReCl_4(CN)_2]\cdot2DMA$ (**1**) and $(DMF)_4MReCl_4(CN)_2$, where M = Mn (**2**), Fe (**3**), Co (**4**)

	1	2	3	4
formula	$C_{42}H_{90}Cl_4N_6O_2Re$	$C_{14}H_{28}Cl_4MnN_6O_4Re$	$C_{14}H_{28}Cl_4FeN_6O_4Re$	$C_{14}H_{28}Cl_4CoN_6O_4Re$
formula wt	1039.22	727.37	728.27	731.36
T, K	139	149	100	155
space group	$P\bar{1}$	$P\bar{1}$	$P\bar{1}$	$P\bar{1}$
Z	1	2	2	2
a, Å	10.5629(8)	9.9185(9)	9.8745(7)	9.957(1)
b, Å	11.9119(9)	10.712(1)	10.5846(7)	10.549(1)
c, Å	12.1271(9)	14.026(1)	13.9378(10)	13.914(1)
α, deg	64.8130(10)	68.07(1)	68.131(4)	67.882(1)
β, deg	75.0150(10)	77.78(1)	78.315(4)	86.275(1)
γ, deg	82.1510(10)	68.91(1)	69.294(4)	69.659(1)
V, Å^3	1333.24(17)	1284.7(2)	1260.38(15)	1266.0(2)
d_{calcd}, g/cm^3	1.294	1.880	1.919	1.919
R1 (wR2), %[b]	3.37 (8.58)	3.66 (9.15)	3.06 (10.26)	4.01 (10.04)

[a] Obtained with graphite-monochromated Mo Kα (λ = 0.710 73 Å) radiation for **1**, **2**, and **4** and Cu Kα radiation (λ = 1.5406 Å) for **3**. [b] R1 = $\sum||F_o| - |F_c||/\sum|F_o|$, wR2 = $\{\sum[w(F_o^2 - F_c^2)^2]/\sum[w(F_o^2)^2]\}^{1/2}$.

X-ray analysis. Absorption spectrum (MeCN): λ_{max} (ε_M) 325 (sh), 348 (4000), 362 (3200), 371 (sh), 391 (1550), 613 (3.05), 672 (2.70), 723 (3.35), 740 (2.98). IR: ν_{CN} 2120 cm^{-1}. ES$^-$-MS (MeCN): m/z 623 ({$(Bu_4N)[ReCl_4(CN)_2]$}$^-$). Anal. Calcd for $C_{42}H_{90}Cl_4N_6O_2Re$: C, 48.54; H, 8.73; N, 8.09. Found: C, 48.78; H, 8.83; N, 8.06.

$(DMF)_4MnReCl_4(CN)_2$ (2). A solution of $Mn(ClO_4)_2\cdot6H_2O$ (0.045 g, 0.13 mmol) in 1.5 mL of DMF was added to a solution of **1** (0.051 g, 0.049 mmol) in 1.5 mL of DMF. The resulting yellow solution was allowed to stand for 8 h to afford yellow plate-shaped crystals. The crystals were collected by filtration, washed with successive aliquots of DMF (3 × 1 mL), THF (3 × 5 mL), and Et_2O (3 × 5 mL), and dried in air to yield 0.030 g (83%) of product. IR: ν_{CN} 2148 cm^{-1}. Anal. Calcd for $C_{14}H_{28}Cl_4MnN_6O_4Re$: C, 23.14; H, 3.89; N, 11.57. Found: C, 23.53; H, 4.06; N, 11.59.

$(DMF)_4FeReCl_4(CN)_2$ (3). A solution of $Fe(ClO_4)_2\cdot6H_2O$ (0.020 g, 0.055 mmol) in 1 mL of DMF was added to a solution of **1** (0.030 g, 0.035 mmol) in 1 mL of DMF. The resulting deep blue solution was allowed to stand for 24 h to afford blue plate-shaped crystals. The crystals were collected by filtration, washed with successive aliquots of DMF (3 × 1 mL), THF (3 × 2 mL), and Et_2O (3 × 2 mL), and dried in air to yield 0.014 g (55%) of product. IR: ν_{CN} 2143 cm^{-1}. Due to the instability of crystals of **3** outside their mother liquor, acceptable elemental analysis has not yet been obtained.

$(DMF)_4CoReCl_4(CN)_2$ (4). A solution of $Co(NO_3)_2\cdot6H_2O$ (0.061 g, 0.11 mmol) in 1.5 mL of DMF was added to a solution of **1** (0.061 g, 0.071 mmol) in 1.5 mL of DMF. The resulting orange solution was allowed to stand for 24 h to afford orange plate-shaped crystals. The crystals were collected by filtration, washed with successive aliquots of DMF (3 × 1 mL), THF (3 × 5 mL), and Et_2O (3 × 5 mL), and dried in air to yield 0.038 g (72%) of product. IR: ν_{CN} 2151 cm^{-1}. Anal. Calcd for $C_{14}H_{28}Cl_4CoN_6O_4Re$: C, 23.01; H, 3.86; N, 11.51. Found: C, 23.41; H, 4.08; N, 11.36.

$(DMF)_4NiReCl_4(CN)_2$ (5). A solution of $Ni(ClO_4)_2\cdot6H_2O$ (0.032 g, 0.088 mmol) in 1.5 mL of DMF was added to a solution of **1** (0.041 g, 0.039 mmol) in 1.5 mL of DMF. The resulting green solution was allowed to stand for 12 days to afford a pale green microcrystalline solid. The solid was collected by filtration, washed with successive aliquots of THF (2 × 10 mL) and Et_2O (2 × 10 mL), and dried in air to yield 0.021 g (75%) of product. IR: ν_{CN} 2148 cm^{-1}. Anal. Calcd for $C_{14}H_{28}Cl_4N_6NiO_4Re$: C, 23.04; H, 3.87; N, 11.53. Found: C, 23.44; H, 4.18; N, 11.43.

X-ray Structure Determinations. Single crystals of compounds **1**−**4** were coated with Paratone-N oil and mounted on glass fibers or Kaptan loops. The crystals were then quickly transferred to a Siemens SMART, Bruker APEX, or Bruker MICROSTAR diffractometer and cooled in a stream of nitrogen gas. Preliminary cell data were collected, giving unit cells consistent with the triclinic Laue groups for all compounds, using the SMART[15] or APEX2[16] program package. The unit cell parameters were later refined against

all data. A full hemisphere of data was collected for each compound. None of the crystals showed significant decay during data collection. Data were integrated and corrected for Lorentz and polarization effects using SAINT[17] and were corrected for absorption effects using SADABS.[18]

Space group assignments were based upon systematic absences, E statistics, and successful refinement of the structures. Structures were solved by direct methods and expanded through successive difference Fourier maps. They were refined against all data using the SHELXTL program.[19] Thermal parameters for all non-hydrogen atoms were refined anisotropically in all compounds, with the exception of C1 in **3**, which was refined isotropically. Table 1 summarizes the unit cell and structure refinement parameters for compounds **1**−**4**.

Magnetic Susceptibility Measurements. Magnetic data were collected using a Quantum Design MPMS-XL SQUID magnetometer. Measurements for **1** and dc susceptibility measurements for **2**−**5** were obtained for finely ground microcrystalline powders restrained in a frozen eicosane matrix within polycarbonate capsules. These measurements were collected in the temperature range 1.8−300 K under a dc field of 1000 Oe. M vs H and ac susceptibility measurements for **2**−**5** were obtained for crystals restrained in frozen mother liquors within sealed quartz tubes to prevent sample decomposition. The field dependences of the magnetization were measured at 1.8 K while sweeping the magnetic field between −7 and 7 T. ac magnetic susceptibility data were collected in zero dc field in the temperature range 1.7−100 K, under an ac field of 4 Oe, oscillating at frequencies in the range 0.5−1488 Hz. All data were corrected for diamagnetic contributions from the sample holder and eicosane, as well as for the core diamagnetism of each sample (estimated using Pascal's constants). The coherence of the collected data for all the compounds was checked between the different techniques of measurements.

Other Physical Measurements. Absorption spectra were measured with a Hewlett-Packard 8453 spectrophotometer. Infrared spectra were obtained on a Nicolet Avatar 360 FTIR or Perkin-Elmer Spectrum 100 Optica FTIR spectrometer, each equipped with an attenuated total reflectance accessory. Carbon, hydrogen, and nitrogen analyses were obtained from the Microanalytical Laboratory of the University of California, Berkeley. X-ray powder

(15) *SMART Software Users Guide, Version 5.1*; Bruker Analytical X-Ray Systems: Madison, WI, 1999.
(16) APEX2 v.2009; Bruker Analytical X-Ray Systems, Madison, WI, 2009.
(17) *SAINT Software Users Guide, Version 7.0*; Bruker Analytical X-Ray Systems: Madison, WI, 1999.
(18) Sheldrick, G. M. SADABS, Version 2.03; Bruker Analytical X-Ray Systems, Madison, WI, 2000.
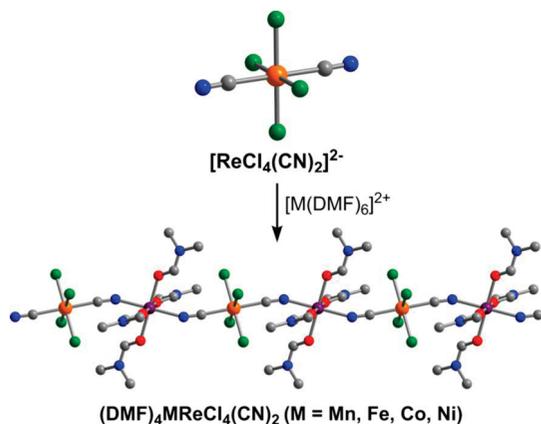(19) Sheldrick, G. M. SHELXTL, Version 6.12; Bruker Analytical X-Ray Systems, Madison, WI, 2000.

Figure 1. Reaction of *trans*-[ReCl$_4$(CN)$_2$]$^{2-}$ (upper) with [M(DMF)$_6$]$^{2+}$ (M = Mn, Fe, Co, Ni) to form the one-dimensional solids (DMF)$_4$MReCl$_4$(CN)$_2$. Orange, purple, green, red, blue, and gray spheres represent Re, M, Cl, O, N, and C atoms, respectively; H atoms have been omitted for clarity. In the structure of **1**, the [ReCl$_4$(CN)$_2$]$^{2-}$ complex resides on a crystallographic inversion center. Selected interatomic distances (Å) and angles (deg): Re−C = 2.148(4), Re−Cl = 2.351(1), 2.341(1), C−N = 1.123(5); Re−C−N = 177.2(3), C−Re−C = 180, C−Re−Cl = 89.6(1), 90.4(1), Cl−Re−Cl = 89.9(1), 90.1(1).

diffraction data were collected using Cu Kα (λ = 1.5406 Å) radiation on a Siemens D5000 diffractometer.

Results and Discussion

Synthesis, Structure, and Magnetic Properties of [ReCl$_4$-(CN)$_2$]$^{2-}$. The complex [ReCl$_4$(CN)$_2$]$^{2-}$ was synthesized via addition of excess (Bu$_4$N)CN to a solution of ReCl$_4$(THF)$_2$ in DMF. Adding water to the solution gave a pale brown precipitate, and diffusion of diethyl ether vapor into a DMA solution of the solid subsequently afforded pale blue rod-shaped crystals of (Bu$_4$N)$_2$[*trans*-ReCl$_4$(CN)$_2$]·2DMA (**1**). X-ray analysis of a single crystal revealed an octahedral coordination geometry for the Re^{IV} center, which is ligated by four equatorial chloride ligands and two axial cyanide ligands oriented trans to one another (see Figure 1). In the structure, the Re atom resides on an inversion center and the C−Re−Cl and Cl−Re−Cl bond angles are close to 90°. The Re−C distance of 2.148(4) Å is slightly longer than those observed for [Re(CN)$_7$]$^{3-}$ (2.06(1)−2.12(1) Å),[20] and the mean Re−Cl distance of 2.346(1) Å is close to that found in [ReCl$_6$]$^{2-}$ (2.351 Å).[21] To our knowledge, the only previous examples of structurally characterized transition-metal complexes of the type [MX$_x$-(CN)$_y$]$^{n-}$ (X$^-$ = halide) are octahedral *trans*-[Pt(CN)$_4$X$_2$]$^{2-}$ (X = Cl, Br, I)[22] and square-planar *trans*-[Au(CN)$_2$X$_2$]$^-$.[23] Thus, *trans*-[ReCl$_4$(CN)$_2$]$^{2-}$ represents the first example of a paramagnetic complex with a mixture of halide and cyanide ligands.

Magnetic susceptibility data collected for **1** yield a value of $\chi_M T = 1.27$ cm^3 K/mol at 300 K, corresponding to an $S = ^3/_2$ spin ground state with $g = 1.65$ (see Figure S1). When the temperature is lowered, $\chi_M T$ remains essentially constant to ca. 70 K, before dropping precipitously at lower temperatures. This downturn can be attributed to the presence of magnetic anisotropy. Additionally, the plot of reduced magnetization

Table 2. Selected Mean Interatomic Distances (Å) and Angles (deg) for (DMF)$_4$MReCl$_4$(CN)$_2$, where M = Mn (**2**), Fe (**3**), Co (**4**)

	2	**3**	**4**
Re−C	2.125(1)	2.118(1)	2.134(1)
M−N	2.228(1)	2.155(1)	2.111(1)
M−O	2.181(1)	2.134(1)	2.098(1)
Re−C−N	175.8(1)	175.4(1)	174.7(1)
M−N−C	155.8(1)	158.1(1)	159.4(1)
φ(Re−C)^a	6.3	5.9	5.7
φ(M−N)^a	7.5	7.0	7.1

^{a} Interchain tilt angles, as described in the text.

reveals a series of nonsuperimposable isofield curves, also indicative of significant anisotropy (see Figure S2). To quantify this effect, the isofield data were fit using ANISOFIT 2.0[24] to give a zero-field splitting parameter of $D = -14.4$ cm^{-1}, with $g = 1.66$. The large magnitude of D establishes the highest value yet reported for a metal cyanide complex of any kind and stems from the considerable spin−orbit coupling associated with the heavy Re^{IV} center.

Since possession of a large negative D value serves as a prerequisite for slow relaxation of the magnetization, the foregoing result emphasizes the potential of **1** as a building unit for new single-molecule and single-chain magnets. Indeed, incorporation of the rhenium(IV) complex [Re(CN)$_7$]$^{3-}$ into molecular clusters has already led to the formation of three single-molecule magnets, among them a species exhibiting a relaxation barrier of 33 cm^{-1}, the highest yet observed for a cyano-bridged molecule.[1e,25] One considerable disadvantage to the pentagonal bipyramidal complex [Re(CN)$_7$]$^{3-}$, however, is its propensity to undergo a spontaneous, solvent-assisted one-electron reduction to diamagnetic [Re(CN)$_7$]$^{4-}$ as metal complexes are appended to it.[1e,20] In [ReCl$_4$(CN)$_2$]$^{2-}$, the presence of π-donating chloride ligands serves to stabilize the higher +4 oxidation state of the rhenium center. Indeed, the cyclic voltammogram of **1** shows a single reversible one-electron reduction occurring at $E_{1/2} = -1.45$ V vs Cp$_2$Fe$^{0/+}$ (see Figure S3), a shift to a considerably more negative potential relative to [Re(CN)$_7$]$^{3-}$ ($E_{1/2} = -1.06$ V vs Cp$_2$Fe$^{0/+}$).[20] In addition, even in the event of a one-electron reduction of [ReCl$_4$(CN)$_2$]$^{2-}$, the octahedral coordination environment of the Re^{III} center would render a paramagnetic t$_{2g}^4$ electron configuration.

Syntheses and Structures of the M^{II}Re^{IV}(CN)$_2$ Chain Compounds. The one-dimensional cyano-bridged solids (DMF)$_4$-MReCl$_4$(CN)$_2$ (M = Mn (**2**), Fe (**3**), Co (**4**), Ni (**5**)) were synthesized through the simple addition of a DMF solution containing the appropriate hydrated metal salt to a DMF solution of **1**, as indicated in Figure 1. X-ray analyses showed the compounds to crystallize as an isostructural series in space group $P\bar{1}$ (see Table 1). For **2**−**4**, structures were obtained through single-crystal X-ray diffraction, while powder diffraction data confirm the structure of **5**. The structures consist of one-dimensional chains, wherein each chain is composed of alternating [ReCl$_4$(CN)$_2$]$^{2-}$ and [M(DMF)$_4$]$^{2+}$ units connected via bridging cyanide ligands. The coordination environment of each Re^{IV} center does not deviate significantly from that observed in [ReCl$_4$(CN)$_2$]$^{2-}$, while the geometry at each M^{II} center approximates an octahedron, with O−M−O and N−M−O angles near 90° (see Table 2). Along the sequence from **2** (M = Mn) to **3** (M = Fe) to **4** (M = Co), the mean M−N and M−O

(20) Bennett, M. V.; Long, J. R. *J. Am. Chem. Soc.* **2003**, *125*, 2394.
(21) Adman, E.; Margulis, T. N. *Inorg. Chem.* **1967**, *6*, 210.
(22) Geiser, U.; Anderson, B. A.; Murray, A.; Pipan, C. M.; Rohl, C. A.; Vogt, B. A.; Wang, H. H.; Williams, J. M.; Kang, D. B.; Whangbo, M. H. *Mol. Cryst. Liq. Cryst.* **1990**, *181*, 105.
(23) Muehle, C.; Karpov, A.; Nuss, J.; Jansen, M. *Z. Naturforsch., B: Chem. Sci.* **2004**, *59*, 567.
(24) Shores, M. P.; Sokol, J. J.; Long, J. R. *J. Am. Chem. Soc.* **2002**, *124*, 2279.
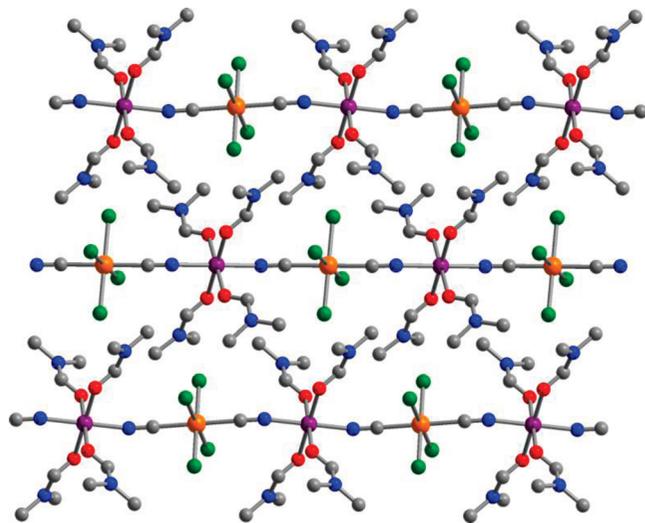(25) These results will appear in a future publication.

Figure 2. Crystal packing diagram for **2**. Orange, purple, green, red, blue, and gray spheres represent Re, Mn, Cl, O, N, and C atoms, respectively; H atoms are omitted for clarity. The closest interchain metal−metal contact is a Re···Mn distance of 7.6845(5) Å.

distances decrease from 2.228(1) and 2.181(1) Å, respectively, to 2.111(1) and 2.098(1) Å, as expected for the decreasing metal ion radii. The Re−C−N angles are all close to 180°, while the M−N−C angles deviate significantly from linearity, with mean angles ranging from 155.8(1)° in **2** to 159.4(1)° in **4**. Such bent angles are not uncommon for M[II] centers coordinated at the nitrogen end of cyanide[1e,20,26] and, in this case, likely arise from the packing of the chains within the crystals. The structure of each solid consists of two crystallographically independent chains, wherein the Re−C bonds on neighboring chains deviate slightly from a parallel orientation and are tilted at angles (φ) ranging from 5.7° to 6.3° relative to each other. Likewise, a similar deviation can be observed between Fe−N bonds on neighboring chains, with tilt angles lying in the range 7.0−7.5°. Despite the minor local tilting relative to one another, both chains propagate along the *b* axis of the crystal (see Figure 2). Compounds **2**−**4** crystallize with no lattice solvent molecules present in the unit cell. Importantly, no close metal−metal contacts are found in the crystal structure, with the shortest interchain metal−metal separations being 7.6845(5), 7.6815(5), and 7.7215(6) Å for **2**−**4**, respectively. In addition, no hydrogen-bonding interactions are evident in any of the structures.

Static Magnetic Properties of the M[II]Re[IV](CN)₂ Chain Compounds. To probe the nature of magnetic exchange interactions in the one-dimensional solids, variable-temperature magnetic susceptibility data were collected for compounds **2**−**5**. A plot of $\chi_M T$ vs T for **2**, collected under an applied dc field of 1000 Oe, is shown in Figure 3. At 300 K, $\chi_M T = 4.79$ cm³ K/mol, slightly lower than the expected value of $\chi_M T = 6.25$ cm³ K/mol for one isolated Re[IV] center ($S = {}^3/_2$) and one isolated Mn[II] center ($S = {}^5/_2$), with $g = 2$. When the temperature is lowered, $\chi_M T$ begins a gradual decrease, reaching a minimum of 2.58 cm³ K/mol at 35 K, before climbing abruptly to a maximum of 19.6 cm³ K/mol at 6 K. This behavior is indicative of antiferromagnetic coupling between the neighboring Re[IV] and

(26) (a) Naumov, N. G.; Artemkina, S. B.; Virovets, A. V.; Fedorov, V. E. *J. Solid State Chem.* **2000**, *153*, 195. (b) Mironov, Y. V.; Fedorov, V. E.; Ijjaali, I.; Ibers, J. A. *Inorg. Chem.* **2001**, *40*, 6320. (c) Brylev, K. A.; Mironov, Y. V.; Naumov, N. G.; Fedorov, V. E.; Ibers, J. A. *Inorg. Chem.* **2004**, *43*, 4833.
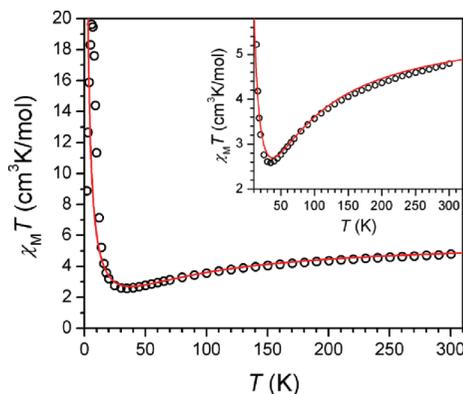
Figure 3. Variable-temperature dc magnetic susceptibility data for **2**, collected in an applied field of 1000 Oe. The solid red line corresponds to a fit to the data, as described in the text. The inset gives a contracted view of the data and fit, highlighting the presence of intrachain antiferromagnetic coupling in **2**.

Mn[II] centers within the chains. Thus, antiferromagnetic exchange overwhelms the competing ferromagnetic interactions, as expected for superexchange through cyanide between Re[IV] (t_{2g}^3) and high-spin Mn[II] ($t_{2g}^3 e_g^2$) centers.[27] The noncompensation of the spins induces a ferrimagnetic arrangement along the chain, giving rise to a repeating unit with $S = 1$. As the temperature drops below 6 K, $\chi_M T$ turns down sharply, owing to field saturation of the magnetization and the magnetic anisotropy of the Re[IV] centers.

In order to quantify the strength of intrachain exchange coupling in **2**, the $\chi_M T$ vs T data were modeled according to the following spin Hamiltonian for a chain comprised of alternating Heisenberg classical spins:

$$H = -2J \sum_{i=1}^{N} (S_i s_i + s_i S_{i+1}) \tag{1}$$

The data were fit (solid red line in Figure 3) in the temperature range 14−300 K, employing an expression previously used to describe the magnetic susceptibility of an alternating chain,[28] to give $J = -5.4(4)$ cm⁻¹, $g_{Re} = 1.80(6)$, and $g_{Mn} = 1.96(2)$.

(27) (a) Entley, W. R.; Trentway, C. R.; Girolami, G. S. *Mol. Cryst. Liq. Cryst.* **1995**, *273*, 153. (b) Weihe, H.; Güdel, H. U. *Comments Inorg. Chem.* **2000**, *22*, 75.
(28) (a) Drillon, M.; Coronado, E.; Beltran, D.; Georges, R. *Chem. Phys.* **1983**, *79*, 449. (b) Georges, R.; Borras-Almenar, J. J.; Coronado, E.; Curely, J.; Drillon, M. *Magnetism: Molecules to Materials I: Models and Experiments*; Miller, J. S., Drillon, M., Eds,; Wiley-VCH: Weinheim, Germany, 2002. The expression used to describe the magnetic susceptibility is as follows:

$$\chi_0 = \frac{N_A \mu_B^2}{6 k_B T} \left[(M_a + M_b)^2 \frac{1+P}{1-P} + (M_a - M_b)^2 \frac{1-P}{1+P} \right]$$

where

$$M_i = g_i \sqrt{S_i(S_i + 1)}$$

$$P = \coth\left(\frac{2J\sqrt{S_a(S_a + 1)S_b(S_b + 1)}}{k_B T} \right) - \left(\frac{k_B T}{2J\sqrt{S_a(S_a + 1)S_b(S_b + 1)}} \right)$$
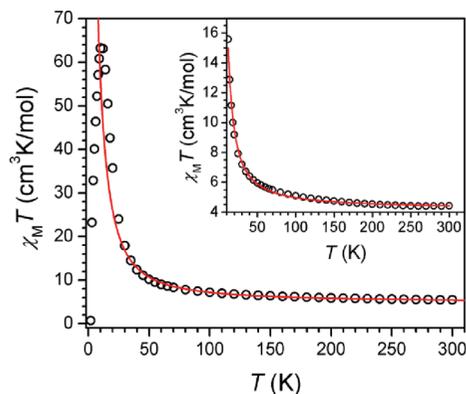
$$S_a = S_{Re}$$

$$S_b = S_M$$

Figure 4. Variable-temperature dc magnetic susceptibility data for **3**, collected in an applied field of 1000 Oe. The solid red line corresponds to a fit to the data, as described in the text. The inset gives a contracted view of the data and fit, highlighting the presence of intrachain ferromagnetic coupling in **3**.

The $\chi_M T$ product for **3** shows distinctly different temperature dependence than does that of **2**, as shown in Figure 4. At 300 K, $\chi_M T$ is 5.46 cm³ K/mol, close to the expected value of $\chi_M T$ = 4.88 cm³ K/mol for one isolated Re^{IV} center ($S = {}^3/_2$) and one isolated high-spin Fe^{II} center ($S = 2$) with $g = 2.00$. As the temperature is lowered, $\chi_M T$ begins to rise, gradually at first, and then abruptly below 40 K, to attain a maximum value of 63.1 cm³ K/mol at 12 K, before dropping sharply at lower temperature. This increase with decreasing temperature is indicative of ferromagnetic coupling between neighboring Re^{IV} ($t_{2g}{}^3$) and Fe^{II} ($t_{2g}{}^4 e_g{}^2$) centers within the chains. The $\chi_M T$ vs T data were modeled similarly to those for **2**, in the temperature range 25–300 K, to give $J = +4.8(4)$ cm⁻¹ and $g = 1.96(6)$.[29] The occurrence of ferromagnetic coupling is somewhat unexpected, given that the antiferromagnetic interactions tend to dominate over the ferromagnetic interactions in such situations.[27] The result is likely associated with the significantly bent Fe–N–C angles of 156.3(1) and 159.7(1)°, which acts to decrease overlap of the $3d_{xz}$ and $3d_{yz}$ orbitals (where z is along the N–Fe–N axis) of the iron with the π^* orbital of cyanide, thereby promoting a net ferromagnetic superexchange pathway. This shift to ferromagnetic coupling likely does not occur in **2** due to the extra unpaired electron in a π-type orbital of Mn, which acts to further promote the antiferromagnetic interaction.

The plot of $\chi_M T$ vs T for **4** follows a trend similar to that observed for **3** (see Figure S4). At 300 K, $\chi_M T = 4.72$ cm³ K/mol, slightly higher than the expected value of $\chi_M T = 3.75$ cm³ K/mol for one isolated Re^{IV} center ($S = {}^3/_2$) and one isolated high-spin Co^{II} center ($S = {}^3/_2$) with $g = 2.00$. This high value is mainly the result of unquenched orbital angular momentum associated with the Co^{II} centers. As the temperature is lowered, $\chi_M T$ increases to a maximum value of 35.8 cm³ K/mol at 6 K, before dropping precipitously below 6 K. The increase in $\chi_M T$ with decreasing temperature is indicative of intrachain ferromagnetic coupling between Re^{IV} ($t_{2g}{}^3$) and Co^{II} ($t_{2g}{}^5 e_g{}^2$) centers. Indeed, a fit to the data in the temperature range 12–300 K confirms a ferromagnetic interaction, with $J = +2.4(1)$ cm⁻¹ and $g = 2.11(3)$. In view of the ferromagnetic coupling in **3**, it is not surprising to observe a similar interaction here, as the Co^{II} center houses one less unpaired electron in a π-type orbital.
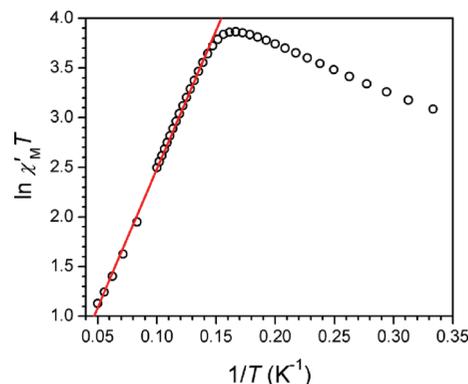

Figure 5. Plot of $\ln(\chi'_M T)$ vs $1/T$ (where χ'_M is the molar component of the ac susceptibility) for **2**, collected in zero applied dc field. The solid red line corresponds to a fit to the linear portion of the data, giving $\Delta_\xi = 19$ cm⁻¹.

Similarly, susceptibility data collected for **5** confirm the presence of intrachain ferromagnetic coupling, as expected between metals with $t_{2g}{}^3$ and $t_{2g}{}^6 e_g{}^2$ configurations, for which the unpaired electrons reside in orthogonal orbitals (see Figure S5). A fit to the data for **5** in the temperature range 14–300 K afforded parameters of $J = +3.7(3)$ cm⁻¹ and $g = 2.04(4)$.

For any one-dimensional classical system, the $\chi_M T$ product in zero applied field is directly proportional to the correlation length, ξ, in zero applied field. In the particular case of anisotropic Heisenberg or Ising-like one-dimensional behavior, ξ, and thus $\chi_M T$, increases exponentially with decreasing temperature, according to the equation

$$\chi_M T / C \approx \exp(\Delta_\zeta / k_B T) \qquad (2)$$

where C is the effective Curie constant, Δ_ξ is the correlation energy (the energy needed to create a domain wall in the chain), and k_B is the Boltzmann constant.[6f,8,30] Following from this relationship, a plot of $\ln(\chi_M T)$ vs $1/T$ should display a linear region, with the line of best fit exhibiting a slope corresponding to the correlation energy. Thus, to ascertain the one-dimensional nature of **2**, variable-temperature ac susceptibility data were collected in the absence of an applied dc field, with an ac field of 4 Oe oscillating at 1 Hz. Indeed, the resulting plot of $\ln(\chi'_M T)$ vs $1/T$ features a linear region in the temperature range 6.8–20 K (see Figure 5), yielding $\Delta_\xi = 19$ cm⁻¹, a value corresponding to the energy required to create a domain wall within the chain. Below 6.8 K, $\ln(\chi'_M T)$ reaches a maximum and then undergoes a linear decrease with decreasing temperature. The intersection of the two linear regions, occurring at ca. 6.5 K, corresponds to the crossover temperature (T^*), where the magnetic correlation becomes physically limited by crystalline defects, and temperatures below T^* comprise the finite-size regime. Similarly, the solids **3**–**5** display clear linear regions in $\ln(\chi'_M T)$, followed by downturns as the temperature is decreased (see Figures S6–S8). Linear fits to the high-temperature data provide correlation energies for **3**–**5** of $\Delta_\xi = 28$, 8.5, and 8.8 cm⁻¹, with crossover temperatures of $T^* = 14$, 5.9, and 6.7 K, respectively. For one-dimensional systems falling within the Ising limit, the correlation energy is related to the intrachain coupling strength, J, and constituent spins through the equation $\Delta_\xi = 4|JS_1 S_2|$.[6f] In the case of **2**, considering the value of J obtained from fitting the $\chi_M T$ vs T data, $4|JS_1 S_2| = 81$ cm⁻¹,

---

(29) The $\chi_M T$ vs T data for **3**–**5** were fit applying the constraint $g_{Re} = g_M$; otherwise, the fitting procedure was unable to independently and accurately determine the two g parameters.

(30) Nakamura, K.; Sasada, T. *J. Phys. C: Solid State Phys.* **1978**, *11*, 331.

Table 3. Summary of Magnetic Data for (DMF)$_4$MReCl$_4$(CN)$_2$, where M = Mn (**2**), Fe (**3**), Co (**4**), Ni (**5**)

	J (cm^{-1})	4|JS_1S_2| (cm^{-1})	Δ_ξ (cm^{-1})	Δ_τ (cm^{-1})	H_A (T)	H_{sat} (T)
2	−5.4(4)	81	19	31	23	13−15
3	4.8(4)	58	28	56	18	23−25
4	2.4(1)	22	8.5	17		
5	3.7(3)	22	8.8	20	11	19−21

more than 4 times the experimental value of Δ_ξ. Likewise, comparisons of 4|JS_1S_2| and Δ_ξ for the other solids indicate strong disagreement between values in **3**−**5** (see Table 3). These stark disagreements demonstrate that the compounds do not fall within the Ising limit with sharp domain walls and instead possess the broad domain walls expected when the anisotropy energy is not sufficiently larger than the exchange energy. In this intermediate regime between the Ising and the Heisenberg limits, the Δ_ξ expression is still unknown and thus no direct relation with J and S is evident.

Variable-field magnetization data collected for **2** at 1.8 K between −7 and 7 T reveal complete reversibility of the magnetization (see Figure S9). Notably, the M vs H curve is smooth, with the absence of any kinks, thus eliminating the possibility of a three-dimensional antiferromagnetic ordering transition down to 1.8 K. A dramatically different M vs H curve is observed for **3** at 1.8 K, however, as sweeping the magnetic field between −7 and 7 T reveals significant hysteresis in the magnetization (see Figure 6). Indeed, inspection of the hysteresis loop shows a coercive field of $H_C = 1.0$ T and a remnant magnetization of $M_R = 3.77$ μ_B. This substantial slow dynamics of the magnetization, indicative of a "magnetic memory," demonstrates classical magnetlike behavior in **3**. Finally, variable-field magnetization data collected for **4** and **5** at 1.8 K between −7 and 7 T show complete reversibility of the magnetization, similar to that observed for **2** (see Figures S10 and S11).

Dynamic Magnetic Properties of the M^{II}Re^{IV}(CN)$_2$ Chain Compounds. To probe the dynamics of the magnetization in the one-dimensional coordination solids, the ac magnetic susceptibility was studied as a function of both temperature and frequency. As shown in Figure 7, variable-temperature ac susceptibility measurements for **2** reveal a strong frequency dependence of both in-phase (χ_M') and out-of-phase (χ_M'') components. From the χ_M'' data, relaxation times (τ) were extracted for each peak through the expression $\tau = 1/2\pi\nu$, where ν is the switching frequency of the ac field. Variable-frequency

Figure 7. Variable-temperature in-phase (upper) and out-of-phase (lower) components of the ac magnetic susceptibility data for **2**, collected in a 4 Oe ac field oscillating at frequencies of 0.5 (maroon), 1 (magenta), 10 (cyan), 50 (green), 100 (orange), 300 (purple), 499 (bright green), 700 (blue), 1000 (red), and 1488 Hz (black). The inset gives an Arrhenius plot of the relaxation time, as determined through variable-temperature (red circles) and variable-frequency ac susceptibility (blue triangles) measurements. The solid line corresponds to a linear fit to the data, giving $\Delta_\tau = 31$ cm^{-1}.

Figure 8. Variable-frequency in-phase (top) and out-of-phase (bottom) ac magnetic susceptibility data for **2**, collected in a 4 Oe ac field at temperatures of 2.2 (black), 2.4 (red), 2.6 (green), 2.8 (blue), 3.0 (cyan), and 3.2 K (magenta).
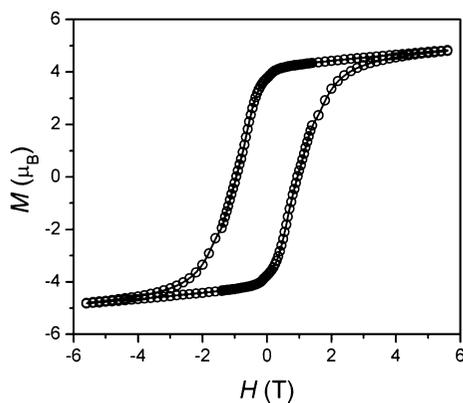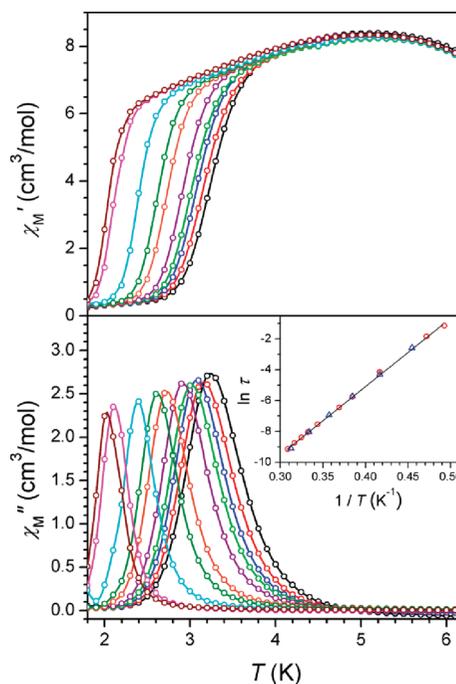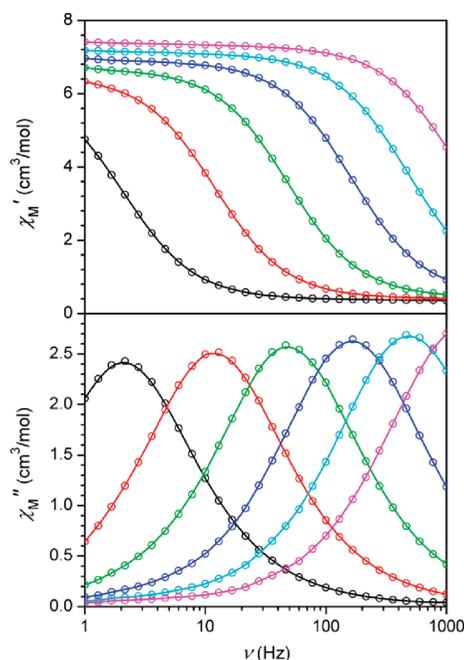
Figure 6. Variable-field magnetization data for **3**, collected at 1.8 K with a mean sweep rate of 150 Oe/min. This plot gives $H_C = 1.0$ T and $M_R = 3.77$ μ_B.

data collected in the temperature range 2.2−3.2 K also show highly frequency-dependent peaks (see Figure 8). Cole−Cole plots of χ_M'' vs χ_M' were constructed from these data (see Figure S12) and were fit to a generalized Debye model to provide

relaxation times at the different temperatures.[31] These fits give α values ranging from 0.12 to 0.18, indicative of a relatively narrow distribution of relaxation times.[31a] For a single-chain magnet, the temperature dependence of the relaxation time should follow an Arrhenius (or thermally activated) behavior, where τ is enhanced exponentially as temperature is decreased.[4,5] Thus, a plot of $\ln(\tau)$ vs $1/T$ should be linear, with the slope being directly proportional to the relaxation energy barrier, Δ_τ. Indeed, the plot of $\ln(\tau)$ vs $1/T$ for compound **2**, with values of τ obtained through both temperature and frequency dependences of the ac susceptibility, demonstrates a clear thermally activated behavior, with a least-squares fit to the line giving $\Delta_\tau = 31$ cm^{-1} and $\tau_0 = 1.3 \times 10^{-10}$ s. The value of τ_0 provides a quantitative estimation of the attempt time of relaxation from the chain bath, and the value obtained here is in good agreement with those found for other reported single-chain magnets.[6] Notably, in the plot of χ_M'' vs T, the magnitude of χ_M'' decreases with decreasing frequency. This likely occurs due to weak antiferromagnetic interchain interactions. Nevertheless, the foregoing analysis of the ac susceptibility, in conjunction with the smooth curve observed in the plot of M vs H, clearly demonstrates the presence of one-dimensional single-chain magnet behavior with no evidence of magnetic order above 1.8 K.

The variable-frequency and variable-temperature ac susceptibility data collected for **3** also demonstrate strong frequency dependence and a corresponding Arrhenius behavior of the relaxation times (Figures S13−S16). However, in comparison to that of **2**, the slow relaxation occurs at higher temperature, resulting in an energy barrier of $\Delta_\tau = 56$ cm^{-1}, with $\tau_0 = 1.0 \times 10^{-10}$ s (and α values in the range 0.21−0.32, indicative of a small distribution of relaxation times). This result is not surprising, given the hysteresis effect observed in the M vs H data for **3** at 1.8 K (see Figure 6). The substantial increase in barrier over the manganese congener likely stems from a combination of larger repeating unit spin ($S = 7/2$ for **3** vs $S = 1$ for **2**) and single-ion anisotropy stemming from unquenched orbital angular momentum in the Fe^{II} ions. This energy for **3** is among the highest for cyano-bridged single-chain magnets yet reported, and the fit to the Arrhenius plot indicates that the compound retains its magnetization for over 1 year at 2 K.[6b,d]

Ac susceptibility data collected for **4** and **5** confirm that both compounds also exhibit slow relaxation of magnetization (Figures S17−S22). Fits to Arrhenius plots derived from Cole−Cole plots for the two compounds give parameters of $\Delta_\tau = 17$ cm^{-1} and $\tau_0 = 2.7 \times 10^{-9}$ s for **4** and $\Delta_\tau = 20$ cm^{-1} and $\tau_0 = 1.7 \times 10^{-9}$ s for **5**. In addition, these fits provide α values in the range 0.19−0.31 for **4** and 0.49−0.63 for **5**, both indicative of distributions of relaxation times.

The dynamics of the magnetization in all solids was observed below their crossover temperatures, meaning that the slow dynamics occurs within the finite-size regime of relaxation.[6f] In this regime, the overall spin-reversal barrier can be expressed as the sum of the correlation and anisotropy energies, as $\Delta_\tau = \Delta_\xi + \Delta_A$.[6f] Having determined both Δ_τ and Δ_ξ values experimentally, the anisotropy energy, Δ_A, can be calculated for each compound, as $\Delta_A = \Delta_\tau - \Delta_\xi$. Within the Ising limit, the anisotropy energy can be easily linked to the anisotropy
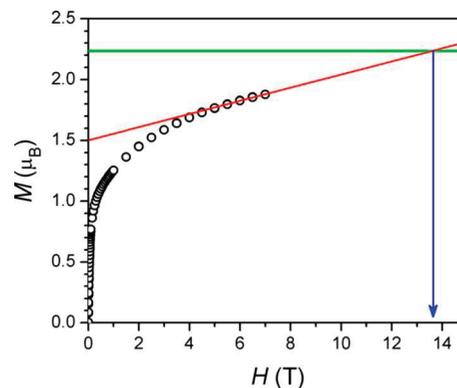

Figure 9. Variable-field magnetization data for **2**, collected at 1.8 K. The solid red line corresponds to a fit to the linear portion of the data, the green horizontal line at $M = 2.23$ μ_B corresponds to the expected magnetization saturation, and the blue vertical line at $H \approx 14$ T denotes the magnitude of the saturation field (H_{sat}).

field, H_A, the field required to induce saturation of the magnetization, through the equation $2\Delta_A = M_{sat}H_A\mu_B$, where M_{sat} is the magnetization at saturation.[7] As shown in Figure 9 and Figures S23 and S24, the saturation of the magnetization cannot be attained experimentally due to the large anisotropy of these systems. Nevertheless, M_{sat} can be determined analytically through the expression $M_{sat} = |g_1S_1 + g_2S_2|/N\mu_B$ for ferromagnetically coupled paramagnetic centers (as in the cases of **3** and **5**) or $M_{sat} = |g_1S_1 - g_2S_2|/N\mu_B$ for antiferromagnetically coupled centers (as in **2**). We note that the calculation of M_{sat} was not possible for **4**, due to the inability to accurately determine the gS product for the Co^{II} ions.[32] Thus, by experimentally determining the anisotropy field for **2**, **3**, and **5** (referred to as H_{sat} to differentiate from the calculated H_A) and then subsequently comparing that value to the calculated H_A, it is possible to confirm that these systems do not fall into the Ising limit, as observed in the dc susceptibility measurements. For instance, the obtained values of $\Delta_\tau = 31$ cm^{-1} and $\Delta_\xi = 19$ cm^{-1} for **2** give $\Delta_A = 12$ cm^{-1}, corresponding to $H_A = 23$ T. A plot of M vs H for **2** at 1.8 K (see Figure 9) reveals the presence of significant magnetic anisotropy, as the magnetization has failed to saturate at fields up to 7 T. Nevertheless, extrapolating the linear portion of the curve to its intersection with the calculated $M_{sat} = 2.2$ μ_B provides $H_{sat} = 13-15$ T.[33] The value of H_{sat} obtained here is clearly much lower than H_A, thereby confirming that **2** does not fall within the Ising limit, consistent with the disagreement between Δ_ξ and $4|JS_1S_2|$. This result demonstrates the lack of an analytical expression for Δ_A, as in the case of Δ_ξ. Similar calculations were made for **3** and **5** using M vs H data (see Figures S23 and S24), and in both cases, poor agreement was found between H_A and H_{sat}, thus indicating non-Ising behavior (see Table 3). These results further highlight the current limitation of the single-chain magnet models when the system does not fall in the Ising limit (i.e.,

(31) (a) Cole, K. S.; Cole, R. H. *J. Chem. Phys.* **1941**, *9*, 341. (b) Boettcher, C. J. F. *Theory of Electric Polarisation*; Elsevier: Amsterdam, 1952. (c) Aubin, S. M.; Sun, Z.; Pardi, L.; Krzystek, J.; Folting, K.; Brunel, L.-J.; Rheingold, A. L.; Christou, G.; Hendrickson, D. N. *Inorg. Chem.* **1999**, *38*, 5329.

(32) Octahedral Co^{II} centers often behave as effective $S_{eff} = 1/2$ systems at low temperature (see references below), and the g value obtained from fitting the χ_MT vs T data used a Co^{II} spin of $S = 3/2$. Thus, a calculation of M_{sat} using that value of g is not physically reliable: (a) Kahn, O. *Molecular Magnetism*; VCH: New York, 1993 and references therein. (b) Plater, M. J.; Foreman, M. R. J.; Coronado, E.; Gómez-García, C. J.; Slawin, A. M. Z. *J. Chem. Soc., Dalton Trans.* **1999**, 4209. (c) Brechin, E. K.; Cador, O.; Caneschi, A.; Cadiou, C.; Harris, S. G.; Parsons, S.; Vonci, M.; Winpenny, R. E. P. *Chem. Commun.* **2002**, 1860.

(33) In our estimation of H_{sat}, we provide a range of fields due to the inherent imprecision in extrapolating the magnetization to its expected saturation.

when the anisotropy energy is significantly smaller than the exchange energy). In this case, analytical expressions for Δ_A, Δ_ξ, and Δ_τ are absent, even while the $\Delta_\tau = 2\Delta_\xi + \Delta_A$ and $\Delta_\tau = \Delta_\xi + \Delta_A$ relations remain valid for any system in its infinite- and finite-size regimes, respectively.[6f] Similar demonstrations were made for **3** and **5** using *M* vs *H* data (see Figures S23 and S24), and in both cases, poor agreement was found between H_A and H_{sat}, confirming their non-Ising single-chain magnet behavior (see Table 3).

Conclusions and Outlook

The foregoing results demonstrate the utility of the new $S = {}^3/_2$, high-anisotropy cyanometalate complex *trans*-$[ReCl_4(CN)_2]^{2-}$ as a building unit for one-dimensional materials that exhibit slow magnetic relaxation. The resulting coordination solids represent the first transmetallic series of cyano-bridged single-chain magnets,[10] enabling a detailed investigation of how adjustment of the exchange coupling and anisotropy via metal-based substitutions affect the relaxation dynamics. Future efforts will focus on extending the coordination chemistry of $[ReCl_4(CN)_2]^{2-}$ to second- and third-row metals, which exhibit large anisotropy stemming from spin−orbit coupling and whose diffuse orbitals promote strong magnetic exchange coupling, in an attempt to isolate one-dimensional solids with increased relaxation barriers. Additionally, extension of this system to copper(II) may also lead to higher barriers, since M−CN−Cu^{II} exchange interactions are known to be considerably stronger than those of other first-row metals.[34] It is our hope that such efforts will result in new single-chain magnets exhibiting large relaxation barriers, opening the way for potential applications at more practical temperatures.

Supporting Information Available: CIF files giving crystallographic data and figures giving additional data. This material is available free of charge via the Internet at http://pubs.acs.org.

JA910963X

(34) (a) Rodríguez-Fortea, A.; Alemany, P.; Alvarez, S.; Ruiz, E.; Scuiller, A.; Decroix, C.; Marvaud, V.; Vaissermann, J.; Verdaguer, M.; Rosenman, I.; Julve, M. *Inorg. Chem.* **2001**, *40*, 5868. (b) Marvaud, V.; Decroix, C.; Scuiller, A.; Guyard-Duhayon, C.; Vaissermann, J.; Gonnet, F.; Verdaguer, M. *Chem. Eur. J.* **2003**, *9*, 1678. (c) Shatruk, M.; Avendano, C.; Dunbar, K. *Prog. Inorg. Chem.*, Ed. Karlin, K. D. Wiley: Amsterdam, 2009 and references therein.